frontiers | Frontiers in Membrane Science and Technology

TYPE Original Research
PUBLISHED 17 March 2025
DOI 10.3389/frmst.2025.1541236

Check for updates

OPEN ACCESS

EDITED BY
Yomen Atassi,
Higher Institute for Applied Sciences and Technology (HIAST), Syria

REVIEWED BY
Bin Liu,
Hunan University, China
Glenn Lipscomb,
University of Toledo, United States

*CORRESPONDENCE
Jong Hak Kim,
jonghak@yonsei.ac.kr

†These authors have contributed equally to this work

RECEIVED 07 December 2024
ACCEPTED 26 February 2025
PUBLISHED 17 March 2025

CITATION
Hwang J, Kang M, Oh NY and Kim JH (2025) Hydrogen-bonded, all-organic pebax/epigallocatechin gallate membranes for CO_2 separation.
Front. Membr. Sci. Technol. 4:1541236.
doi: 10.3389/frmst.2025.1541236

COPYRIGHT
© 2025 Hwang, Kang, Oh and Kim. This is an open-access article distributed under the terms of the Creative Commons Attribution License (CC BY). The use, distribution or reproduction in other forums is permitted, provided the original author(s) and the copyright owner(s) are credited and that the original publication in this journal is cited, in accordance with accepted academic practice. No use, distribution or reproduction is permitted which does not comply with these terms.

Hydrogen-bonded, all-organic pebax/epigallocatechin gallate membranes for CO_2 separation

Junseok Hwang†, Miso Kang†, Na Yeong Oh and Jong Hak Kim*

Department of Chemical and Biomolecular Engineering, Yonsei University, Seoul, Republic of Korea

This study systematically investigates the structural, thermal, mechanical, and gas separation properties of hydrogen-bond (H-bond) induced Pebax/epigallocatechin gallate (EGCG) membranes, emphasizing the role of EGCG as an H-bond inducer. Pebax® 1,657 membranes were fabricated via solution casting using a mixed solvent system of water and ethanol, with EGCG incorporated at varying concentrations (0–20 wt%) to assess its impact on membrane properties. The hydroxyl-rich structure of EGCG facilitates robust hydrogen-bonding interactions with the Pebax matrix, forming a transiently crosslinked structure. This strong interaction reduces the matrix's free volume and alters its microstructure by decreasing the crystalline domain size of polyamide (PA) and enhancing the exposure of the amorphous poly (ethylene oxide) (PEO) chains in Pebax. At an optimal EGCG loading of 5 wt%, the membranes exhibited a CO_2 permeability of 60.2 $\pm$ 1.1 Barrer and a CO_2/N_2 selectivity of 49.6 $\pm$ 0.8, representing a 33% increase in selectivity compared to pristine Pebax membranes. These performance enhancements are attributed to the reduction in fractional free volume (FFV) due to H-bond-induced structural modifications and the increased availability of amorphous PEO chains, which enhance CO_2/N_2 diffusivity selectivity and solubility selectivity, respectively. Moreover, mechanical testing demonstrated that the 5 wt% EGCG-incorporated membrane maintains its mechanical integrity, preserving the tensile strength of pristine Pebax while slightly improving elongation at break. Molecular dynamics (MD) simulations of FFV and solubilities corroborate the experimental observations, offering insights into the mechanisms underlying the improved gas separation performance. The results highlight EGCG as an effective H-bond inducer for tuning the properties of Pebax membranes, achieving an optimal balance between mechanical stability and gas separation efficiency at 5 wt% loading. This study provides a foundation for scaling up all-organic Pebax/EGCG membranes into high-performance membrane structures, presenting a promising approach for industrial CO_2 separation and carbon capture applications.

KEYWORDS

hydrogen bond, Pebax, epigallocatechin gallate, gas separation membrane, molecular dynamics simulation

1 Introduction

The increasing concentration of CO_2 in the atmosphere has intensified the demand for efficient carbon capture technologies (Guiver, 2022). Polymeric membranes have gained attention as a promising solution due to their simplicity, cost-effectiveness, and low environmental footprint (Han and Ho, 2021; Lei et al., 2020). Among these, poly

(ethylene oxide) (PEO)-based membranes are particularly notable for their strong affinity with CO_2, attributed to the ether oxygen in PEO chains, which enhances CO_2 solubility and selectivity (Liu et al., 2013; Kargari and Rezaeinia, 2020). However, the high crystallinity of high-molecular-weight PEO often introduces structural imperfections that limit its gas separation performance (Zhu et al., 2020; Kim, 2022; Kang et al., 2021). Pebax, a poly (ether-block-amide) copolymer, serves as an excellent platform for CO_2 separation by integrating a rigid polyamide (PA) segment for mechanical strength with a flexible poly (ethylene oxide) (PEO) segment that boosts CO_2 separation performance (Kim et al., 2019). However, the crystalline domains in the PA segment hinder gas diffusion, reducing overall permeability and limiting its application scope (Embaye et al., 2021). To address these challenges, researchers have explored the incorporation of organic additives and crosslinking agents, which are prized for their cost-effectiveness, processability, and consistent performance (Zou and Zhu, 2018; Knebel and Caro, 2022; Oh et al., 2025).

Various additives have been employed to improve the gas separation performance of PEO-based membranes. Porous inorganic fillers, such as metal-organic frameworks (MOFs), and porous organic fillers, including covalent organic frameworks (COFs), porous aromatic frameworks (PAFs), have shown great promise for CO_2 separation membranes due to their high surface area, stability, and selectivity. However, their practical application is often hindered by challenges related to complex synthesis and difficulties in large-scale polymer integration (Liu et al., 2021; Thankamony et al., 2019; Wu et al., 2021; Yan et al., 2024; Hao et al., 2014; Hou et al., 2020). Commercial polymers, such as poly (ethylene glycol), poly (acrylic acid), poly (vinyl pyrrolidone), and polytetrafluoroethylene, have also been incorporated as organic additives. These polymers offer advantages like low cost and easy processability but generally exhibit limited separation performance (Kim et al., 2024; Yu et al., 2023; Hyo Jun et al., 2024). Additionally, interaction agents have been used to disrupt the crystallization of PEO chains, enabling high selectivity and simplicity in membrane preparation. Chemically crosslinked membranes, employing agents such as thiols, acrylates, epoxies, and amines, have demonstrated excellent CO_2 selectivity (Kim et al., 2020; Norouzbahari and Gharibi, 2020; Shao and Chung, 2009; Li et al., 2024; Chen et al., 2023). However, these methods often require additional steps, such as heating (Shao and Chung, 2009), UV irradiation (Norouzbahari and Gharibi, 2020; Li et al., 2024), or the removal of unreacted monomers (Chen et al., 2023). In contrast, physical interaction methods based on hydrogen bonding (H-bonds) offer significant advantages due to their straightforward preparation via simple mixing. Studies have explored the incorporation of H-bonding molecules into the PEO matrix, including trehalose dihydrate (Wang et al., 2023), 4-hydroxybenzoic acid (Choi and Kang, 2016), 5-hydroxyisophthalic acid (Yoon and Kang, 2018), 2,4,6-triaminopyrimidine (Oh et al., 2025), and polyalcoholic compounds like maltitol and mannitol (Nobakht and Abedini, 2022a). These molecules effectively disrupt PEO crystallization through strong intermolecular interactions, enhancing gas separation performance.

Epigallocatechin gallate (EGCG), with its eight hydroxyl groups, emerges as a promising alternative to previously studied H-bonding molecules. It offers straightforward processing, excellent compatibility with the Pebax matrix, and improved CO_2-selective permeation through an H-bond-induced crosslinked polymer network. This study marks the first application of EGCG as an H-bonding inducer in Pebax membranes to enhance CO_2 separation performance. By systematically investigating the effects of EGCG on membrane structure, properties, and gas separation efficiency, this research establishes EGCG as a practical and scalable solution for advanced CO_2 separation technologies. Additionally, detailed molecular dynamics (MD) simulations were performed to explore the changes in gas sorption behavior induced by the incorporation of EGCG, providing deeper insights into the mechanism of performance enhancement.

2 Experimental

2.1 Materials

Pebax®1,657, composed of 40 wt% polyamide (PA) and 60 wt% polyether (PEO), was supplied by Arkema, Inc. (Paris, France). Epigallocatechin gallate (EGCG) was procured from Sigma-Aldrich. Deionized (DI) water and ethanol (EtOH) were obtained from Duksan Pure Chemicals Co., Ltd. (Korea). All solvents used were of reagent grade and employed without additional purification.

2.2 Fabrication of blend membranes

The blend membranes were prepared using the solvent-evaporation method. First, a polymer solution was prepared by dissolving Pebax in 5 mL of an EtOH/H_2O mixture (7:3 by volume) at 70°C under vigorous stirring. Separately, various amounts of EGCG (5, 10, 15, and 20 wt% of the total solute mass) were dissolved in 3 mL of the same solvent mixture and sonicated for 30 min. The EGCG solution was then added to the Pebax solution and stirred for an additional 30 min under identical conditions. All solutions were prepared at a concentration of 5 w/v%. The resulting homogeneous mixture was cast onto a Teflon dish and left to dry at room temperature for 24 h to allow slow solvent evaporation. To ensure complete removal of the solvent, the cast membranes were further dried in a drying oven at 50°C for 24 h. The prepared membranes are designated as Pebax/EGCG X%, where X indicates the EGCG weight percentage relative to the total solute mass (5, 10, 15, and 20%, respectively).

2.3 Characterizations

Fourier-transform infrared spectroscopy (FT-IR; Spectrum 100, PerkinElmer, United States) was employed to analyze the chemical structures and interactions within the membranes. The crystallinity and structural properties were examined using high-resolution X-ray diffraction (XRD; Ultima IV, Rigaku, Japan) with Cu-Kα radiation (λ = 1.5406 Å) operated at 45 kV and 200 mA. The morphologies of the membranes were investigated via field-emission scanning electron microscopy (FE-SEM; 7610F-Plus, JEOL, Japan). Thermal properties were analyzed using differential scanning calorimetry (DSC; Discovery DSC, TA Instruments) with a heating rate of 20°C min^{-1} under a nitrogen atmosphere. Thermal

stability was assessed through thermogravimetric analysis (TGA; Discovery TGA, TA Instruments) at a heating rate of 20°C min^{-1} in air. The CO_2 adsorption capacity of the membranes was measured using TGA (TGA 55, TA Instruments) at a constant temperature of 27°C. Mechanical properties, including tensile stress and strain, were evaluated using a universal testing machine (UTM; LR10KPlus Series) with a crosshead speed of 30 mm min^{-1}. For consistency, all specimens were standardized to dimensions of 2 cm × 1 cm.

2.4 Gas separation measurement

The gas permeation properties of the dense polymer membranes were evaluated at 35°C using the time-lag method with a constant volume/variable pressure system (Airrane Co., Ltd., Korea). Each membrane had an active area of 15.2 cm^2. During the measurements, the upstream pressure was maintained at 760 torr, while the downstream pressure was kept below 2 torr. Permeability was calculated by monitoring the pressure increase in the fixed downstream volume and was expressed in barrer units (1 barrer = 1×10^{-10} cm^3(STP) cm cm^{-2} s^{-1} cm Hg^{-1}). The CO_2/N_2 selectivity was determined by taking the ratio of the permeability values for the two gases. To ensure reliability, the average permeability and selectivity values were calculated from three replicate membrane samples.

2.5 Computational methods

The effect of EGCG additives on Pebax membranes was analyzed using Materials Studio 2024, employing the Forcite, Amorphous Cell, and Sorption modules. Each Pebax unit chain comprised 9 PA segments and 35 PEO segments, maintaining a weight ratio of 40:60, as previously reported (Didden et al., 2018). Four of these unit chains were combined to form a Pebax polymer chain with a total molecular weight of 10,418 g/mol. Amorphous cells for Pebax and Pebax/EGCG 5% were constructed with an initial density of 0.1 g/cm^3. The Pebax cell contained five Pebax chains, while the Pebax/EGCG 5% cell included five Pebax chains and six EGCG molecules, corresponding to the weight ratio of the additives. Following cell construction, each amorphous polymer cell was equilibrated using a modified 21-step MD compression and relaxation scheme (Yeh et al., 2023) with additional two isobaric-isothermal ensemble (NPT) steps at 298 K and 1 atm for 1,000 and 5,000 ps. The COMPASSIII force field was utilized to model the molecular interactions, employing the particle-particle particle-mesh (PPPM) method for electrostatic energy summation and atom-based Van der Waals energy summation. These simulation models enabled the investigation of structural and gas sorption properties of the membranes. CO_2 and N_2 loading capacities were calculated using the Sorption task via the Metropolis Monte Carlo method, with atom-based summation for both electrostatic and Van der Waals interaction energies (Sun et al., 2023). The density, FFV, and CO_2 uptake were calculated for different numbers of Pebax chains in an amorphous cell (Supplementary Table S2). While the density and FFV did not change significantly, CO_2 uptake increased as the number of chains increased. The CO_2 uptake remained relatively stable once the number of chains exceeded three, validating the appropriate number of chains in the amorphous cell. The same MD compression and relaxation steps were performed to equilibrate the system. Subsequently, an additional NPT-MD simulation was conducted for 1,000 ns to gather data for physical analysis (Erpenbeck and Wood, 1991). To investigate the intermolecular interactions between gas molecules and functional groups in Pebax, the radial distribution functions (RDFs) of different gas-atom pairs were analyzed. RDF, denoted as g(r), represents the probability of locating an atom at a distance r from a reference atom within an infinitesimally thin spherical shell. This probability is mathematically defined according to the method described by Hansen and McDonald (1990) (Hansen and McDonald). The RDF analysis focused on the interactions between gas molecules and functional groups such as ether oxygen in PEO and nitrogen in PA.

3 Results and discussion

3.1 Interactions and structure of membranes

First, hydrogen-bonding interactions in Pebax/EGCG membranes were investigated using FT-IR spectroscopy (Figure 1a). The FT-IR spectrum of Pebax displayed characteristic absorption bands, including a C=O stretching vibration at 1731 cm^{-1}, a C—O—C stretching band at 1,104 cm^{-1}, and additional bands at 1,637 cm^{-1} and 3,298 cm^{-1} corresponding to the stretching vibrations of H—N—C=O and N—H groups, respectively (Nobakht and Abedini, 2022b; Mohammed et al., 2019; Farashi et al., 2019). For EGCG, the band at 3,352 cm^{-1} was attributed to the hydroxyl (-OH) stretching, while the band at 1,690 cm^{-1} corresponded to ester C=O stretching (Pan et al., 2019; Wang et al., 2019). Upon incorporating EGCG into Pebax, a blue shift in the C=O stretching band of EGCG from 1,690 cm^{-1} to 1709 cm^{-1} was observed, indicating strong intermolecular interactions between EGCG and Pebax. Deconvolution of the C=O stretching bands revealed that the secondary carbonyl band at 1,709 cm^{-1} became more prominent than the primary carbonyl band of Pebax at 1,731 cm^{-1} as EGCG loading increased (Supplementary Figure S1 and Figure 1b). This change in the intensity ratio (I_{1709}/I_{1731}) highlights the strengthening hydrogen bonding interactions between EGCG and the Pebax matrix. Additional spectral shifts in the hydroxyl and amide regions further supported these interactions. Intensity changes in the N—H stretching band at 3,298 cm^{-1} and the -OH stretching band at 3,352 cm^{-1} confirmed hydrogen bonding between EGCG's hydroxyl groups and Pebax's amide groups. A schematic of the proposed hydrogen bonding interactions is shown in Figure 1c, illustrating the key role of EGCG in forming strong intermolecular bonds with Pebax. These hydrogen-bonding interactions play a crucial role in the structural organization of the Pebax/EGCG membranes, which is further analyzed through XRD and DSC.

XRD analysis was performed to assess the crystallinity and structural properties of the Pebax/EGCG membranes (Figure 2a; Supplementary Figure S2; Table 1). In the XRD spectrum of neat Pebax, a strong diffraction peak at $2\theta \approx 24.04^\circ$ corresponds to the crystalline phase of the PA segment ($2\theta_{PA}$), while a broad peak

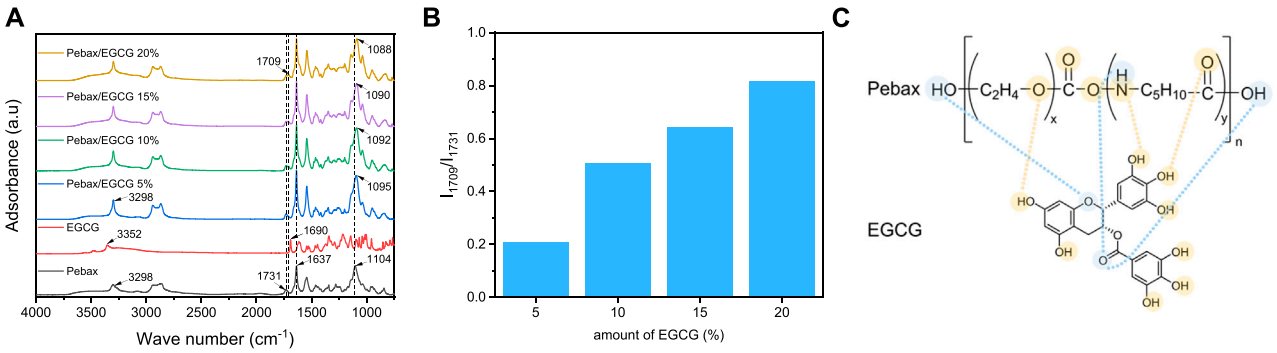

FIGURE 1
(a) FT-IR spectra of Pebax, EGCG, and Pebax/EGCG membranes with various EGCG contents, **(b)** peak intensity ratio between 1,709 cm^{-1} and 1,731 cm^{-1} for various EGCG loadings, **(c)** proposed H-bonding interactions between Pebax and EGCG.

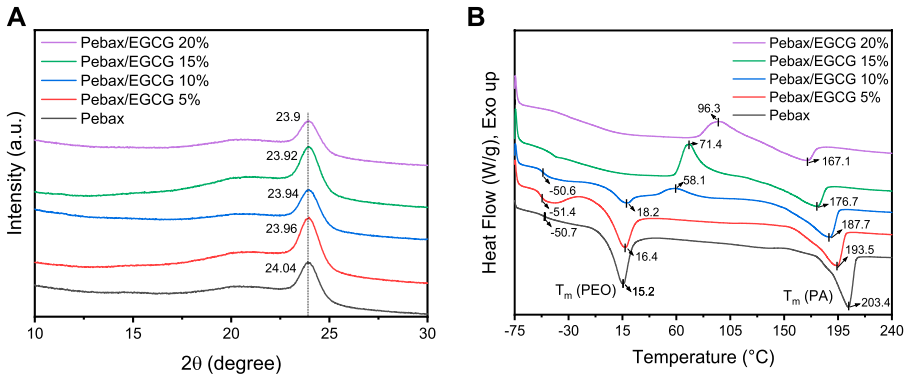

FIGURE 2
(a) XRD patterns and **(b)** DSC thermograms of Pebax and Pebax/EGCG membranes with various EGCG loadings.

TABLE 1 Bragg's angle of PA and PEO, intensity-based crystallinity (%), and size of the crystalline domain of Pebax and Pebax/EGCG membranes with various EGCG contents.

	$2\theta_{PA}$ (degree)	$2\theta_{PEO}$ (degree)	$I_{PA}/I_{PA}+I_{PEO}$ (%)	Size of crystalline domain, τ (nm)
Pebax	24.04	21.38	69	7.2
Pebax/EGCG 5%	23.96	21.49	67	7.0
Pebax/EGCG 10%	23.94	21.40	64	6.9
Pebax/EGCG 15%	23.92	21.51	64	7.1
Pebax/EGCG 20%	23.90	21.48	64	7.0

around $2\theta \approx 21.38^{\circ}$ is associated with the amorphous phase of the PEO segment ($2\theta_{PEO}$). The corresponding d-spacing values, calculated using Bragg's law, are approximately 3.7 Å for the PA segment and 4.15 Å for the PEO segment. With the incorporation of EGCG, the position of the $2\theta_{PA}$ peak remained nearly unchanged regardless of the EGCG content.

To further investigate the impact of EGCG on the membrane crystallinity, XRD spectra of both Pebax and Pebax/EGCG membranes were deconvoluted (Supplementary Figure S2). The intensity-based crystallinity was calculated using the following equation:

$$\frac{I_{PA}}{I_{PA}+I_{PEO}}$$

where I_{PA} is the peak intensity of the diffraction peak of the crystalline PA segment, and I_{PEO} corresponds to the amorphous PEO region. Additionally, the size of the PA crystalline domain (τ) was determined using the Scherrer equation:

TABLE 2 Melting temperature, crystallization temperature and degree of crystallinity of Pebax and Pebax/EGCG membranes with different EGCG loadings.

	T_g (°C) (PEO)	T_m (°C) (PEO)	T_m (°C) (PA)	T_{cc} (°C) (PA)	ΔH_m		$X_{c,PEO}$ (%)	$X_{c,PA}$ (%)
					PEO	PA		
Pebax	−50.7	15.2	203.4	—	26.0	28.3	26.0	30.8
Pebax/EGCG 5%	−51.4	16.4	193.5	—	22.2	24.2	23.5	27.6
Pebax/EGCG 10%	−50.6	18.2	187.7	58.1	11.0	24.8	12.3	30.0
Pebax/EGCG 15%	—	—	176.7	71.37		20.8	—	26.5
Pebax/EGCG 20%	—	—	167.1	96.28		13.9	—	18.9

$$\tau = \frac{K\lambda}{\beta \cos\theta}$$

where τ is the crystalline domain size, K is the dimensionless shape factor (typically 0.9), λ is the wavelength, β is the full-width at half-maximum (FWHM) of the diffraction peak in radians, and θ is the Bragg angle.

As shown in Table 1, the intensity-based crystallinity decreased from 69% to 64% (10% EGCG incorporation) but remained largely unchanged with EGCG incorporation up to 20%. This change in crystallinity indicates that the PA chain packing is minimally disrupted at low EGCG loadings, an essential factor for maintaining the membrane's ductility and structural integrity. Additionally, the incorporation of EGCG slightly reduced the size of the PA crystalline domains (τ). This reduction suggests that the outer regions of the PA crystalline domains are disrupted due to hydrogen-bonding interactions between EGCG and the polymer matrix. These findings highlight that at low concentrations, EGCG acts as a hydrogen-bonding inducer without compromising the crystallinity or structural integrity of the Pebax membranes, ensuring their mechanical robustness and performance stability.

Differential Scanning Calorimetry (DSC) analysis was performed to examine the thermal transitions, including the glass transition temperature (T_g), cold crystallization temperature (T_{cc}), and melting temperature (T_m) of Pebax/EGCG membranes (Figure 2b; Table 2). The DSC samples were initially heated in a nitrogen atmosphere at a rate of 20°C/min from −75°C to 250°C, then rapidly cooled back to −75°C. Subsequently, the samples were reheated to 250°C at the same rate, and the thermal transitions were analyzed using the second heating cycle. For neat Pebax, a single T_g was observed at −50.7°C, corresponding to the soft PEO phase, with no detectable T_g for the PA phase due to its low chain mobility. Up to 10% EGCG loading, the T_g of the PEO phase remained almost unchanged, indicating that low EGCG content does not significantly affect PEO chain mobility. The neat Pebax membrane exhibited strong endothermic peaks at 15.2°C and 203.4°C, representing the T_m of the soft PEO and hard PA phases, respectively, consistent with the microphase-separated morphology of the block copolymer (Thanakkasaranee et al., 2018). When 5% and 10% EGCG were incorporated, the T_m of the PEO phase increased to 16.4°C and 18.2°C, respectively, suggesting that favorable H-bond-induced interaction between EGCG and PEO chains restrict the mobility of chains, thereby enhancing the thermal stability of PEO domain. This trend (distinct T_m increase in PEO) is consistent with similar study on Pebax/polyalcohol blends (Nobakht and Abedini, 2022a). Conversely, the T_m of the PA phase decreased to 193.5°C and 187.7°C, suggesting that hydrogen bonding between EGCG and PA chains was weaker compared to its interaction with PEO. Moreover, the decrease in the T_m of the PA phase with EGCG incorporation can be attributed to the reduction in the PA crystalline domain size (τ), as highlighted in the XRD analysis. At higher EGCG loadings, the T_m of the PEO phase disappeared, indicating that the PEO segments became fully amorphous due to disruption of chain packing by the increased EGCG content. Meanwhile, the T_m for the PA phase remained, further supporting the preferential interaction of EGCG with the PEO segments.

Incomplete crystallization during cooling can lead to cold crystallization upon reheating (T_{cc}; cold crystallization temperature) due to slow crystallization kinetics (Yin et al., 2015; Gao et al., 2021). In the second heating cycles of samples with 10%, 15%, and 20% EGCG incorporation, T_{cc} of the PA phase was observed in the range of 58°C–96°C, confirming incomplete crystallization during cooling scans. Previous studies have reported the crystallization temperature (T_c) of PA at 189.7°C and its T_{cc} at 69.9°C (Liu et al., 2003), significantly lower than the typical T_c. As shown in Supplementary Figure S3, the cooling scans of Pebax and Pebax/EGCG reveal that $T_{c,PA}$ of Pebax progressively decreases with increasing EGCG content, eventually disappearing in the cooling scans of Pebax/EGCG 15% and 20%. This demonstrates that H-bonding interactions between EGCG and the PA phase hinder crystallization during the cooling process, resulting in the emergence of T_{cc}. Furthermore, T_{cc} increases as EGCG content rises, reflecting that higher EGCG concentrations further slow down the crystallization kinetics, necessitating additional heat input to achieve crystallization. Consequently, EGCG significantly disrupts the crystallization behavior of the PA phase and reduces the T_m of PA segments. To further understand the structural properties of the membranes, the degree of crystallinity for the PEO ($X_{c,PEO}$) and PA ($X_{c,PA}$) domains was calculated using the following equation:

$$X_{c,i} = \frac{\Delta H_{m,i}}{w_i \Delta H^{\circ}_{m,i}} \times 100\ (\%)$$

where $\Delta H_{m,i}$ is the heat of melting of the microphase crystals evaluated by the integrated areas under each melting peak, w_i is the weight fraction of each domain, and $\Delta H^{0}_{m,i}$ is the heat of melting of the fully crystalline phase. The values of $\Delta H^{\circ}_{m,PEO}$ and $\Delta H^{\circ}_{m,PA}$ have been reported in previous studies as 166.4 and 230.0 J/g, respectively (Kim et al., 2019; Nobakht and Abedini, 2022a;

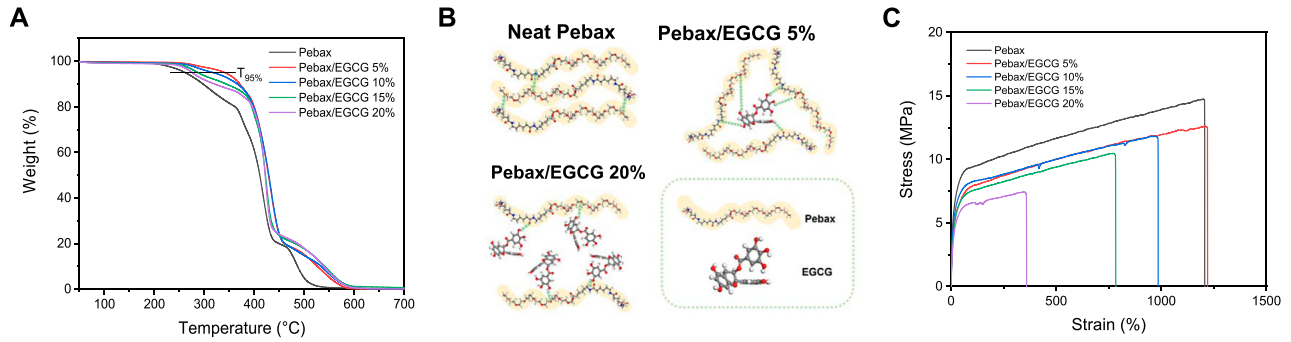

FIGURE 3
(a) TGA curves of Pebax and Pebax/EGCG membranes with various EGCG loadings, **(b)** schematic illustration of proposed hydrogen bonding interactions in neat Pebax and Pebax/EGCG membranes, and **(c)** stress-strain curves of Pebax and Pebax/EGCG membranes with various EGCG loadings.

Rabiee et al., 2015). As shown in Table 2, $X_{c,PA}$ does not significantly decrease with increasing EGCG content up to 15%, while $X_{c,PEO}$ decreases markedly. This suggests that the hydroxyl groups of EGCG interact more favorably with PEO phase, disrupting the van der Waals (VdW) interactions between adjacent PEO chains and ultimately hindering the crystallization of the PEO chains. The combination of a relatively stable PA crystalline domain and an amorphous PEO domain resulting from EGCG incorporation is advantageous for CO_2 separation. The increased amorphous regions in the PEO phase can improve CO_2 permeability and selectivity, while the stable PA crystalline regions ensure the membrane's mechanical integrity.

3.2 Thermal and mechanical properties of membranes

TGA was performed to assess the thermal stability of Pebax/EGCG membranes (Figure 3a). The TGA curves of neat Pebax exhibited a single degradation phase with a one-step decomposition profile. Upon EGCG incorporation, the onset of thermal degradation shifted to slightly higher temperatures, indicating enhanced thermal stability of the polymer matrix. The thermal degradation temperature (T_d), or $T_{95\%}$, which represents the temperature at which 5% weight loss occurs, was approximately 270°C for neat Pebax. In contrast, the incorporation of EGCG raises the $T_{95\%}$, with the Pebax/EGCG 5% membrane demonstrating the highest thermal stability, retaining weight up to approximately 370°C. At low EGCG concentrations (e.g., 5 wt%), multiple strong hydrogen bonds formed between EGCG and the functional groups of the polymer, creating a thermally stable composite membrane. These hydrogen-bonding interactions restricted polymer chain mobility, contributing to the enhanced thermal stability of the membrane. A schematic representation in Figure 3b illustrates how EGCG molecules are uniformly distributed within the polymer matrix, forming multiple interaction sites. However, at higher EGCG loadings (e.g., 20 wt %), the excess EGCG disrupted van der Waals and hydrogen-bonding interactions among the Pebax polymer chains, leading to reduced thermal stability compared to the optimal 5 wt% EGCG membrane. This trend highlights the critical importance of optimizing EGCG content to maintain strong interactions between the additive and the polymer matrix. Furthermore, minimal weight loss was observed for all membranes below 270°C, confirming their suitability for applications in post-combustion carbon capture, where flue gas temperatures typically range from 110°C to 140°C (Ren et al., 2012).

The mechanical properties of Pebax/EGCG membranes were evaluated using stress-strain curves (Figure 3c). Neat Pebax demonstrated remarkable flexibility, with an elongation at break exceeding 1,400%, reflecting its high ductility, and a tensile stress at break of 15 MPa. Upon incorporating 5% EGCG, the membrane's elongation at break further increased, indicating enhanced flexibility due to improved chain mobility. This observation aligns with the DSC results, which showed a decrease in T_g with 5% EGCG loading. However, the tensile stress at break slightly decreased, likely attributed to a reduction in crystallinity, as evidenced by the DSC analysis. As the EGCG concentration increased to 10%, 15%, and 20%, both the elongation at break and tensile stress at break gradually declined. This reduction suggests that excessive EGCG disrupts chain entanglement and compromises the membrane's mechanical performance. These findings emphasize the critical need for optimizing EGCG content. While low levels of EGCG enhance flexibility and maintain mechanical stability, excessive loading diminishes ductility and tensile strength, adversely affecting the overall performance of the membranes.

Surface and cross-sectional SEM images of neat Pebax and Pebax/EGCG membranes were analyzed to evaluate the impact of EGCG on membrane morphology (Supplementary Figure S4). The surface of the pristine Pebax membrane displayed a distinctive structure characterized by nanofibril-like PA crystalline domains embedded within amorphous PEO regions, consistent with its microphase-separated morphology (Kim et al., 2024). With the addition of EGCG, the surface morphology underwent noticeable changes, with a reduction in visible nanofibrils of PA. This suggests that EGCG interacts with and modifies the crystalline structure of PA, a finding supported by the XRD and DSC analyses. Cross-sectional SEM images of both pristine Pebax and Pebax/EGCG

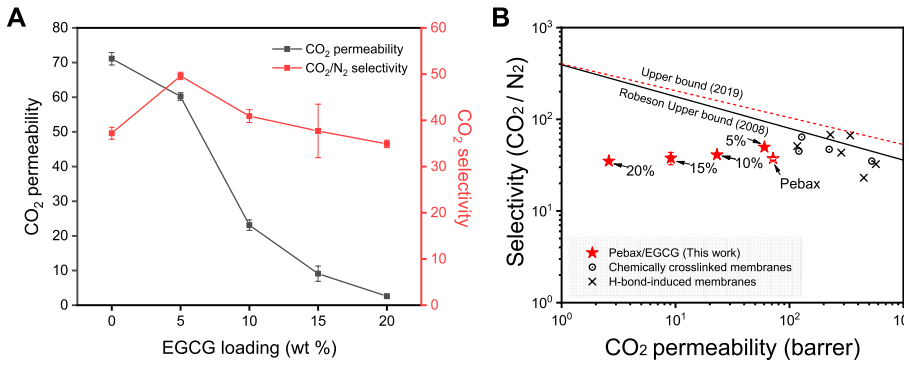

FIGURE 4
(a) CO_2 permeabilities and CO_2/N_2 selectivities of Pebax and Pebax/EGCG membranes with various EGCG loadings and **(b)** a plot of CO_2 permeability *versus* CO_2/N_2 selectivity for pristine Pebax, Pebax/EGCG membranes, and other PEO-based crosslinked or hydrogen bonded membranes previously reported in the literature.

TABLE 3 Pure gas separation performance and thickness of Pebax, and Pebax/EGCG membranes at 1bar, 35°C.

	Thickness (μm)	CO_2 Permeability (barrer)	N_2 permeability (barrer)	Selectivity (CO_2/N_2)
Neat Pebax	105	71.7 ± 1.8	1.9 ± 0.1	37.2 ± 1.3
Pebax/EGCG 5%	100	60.2 ± 1.1	1.2 ± 0.04	49.6 ± 0.8
Pebax/EGCG 10%	95	23.1 ± 1.5	0.6 ± 0.09	40.9 ± 1.4
Pebax/EGCG 15%	90	9.1 ± 2.2	0.3 ± 0.08	37.7 ± 5.8
Pebax/EGCG 20%	90	2.6 ± 0.4	0.07 ± 0.01	34.9 ± 0.8

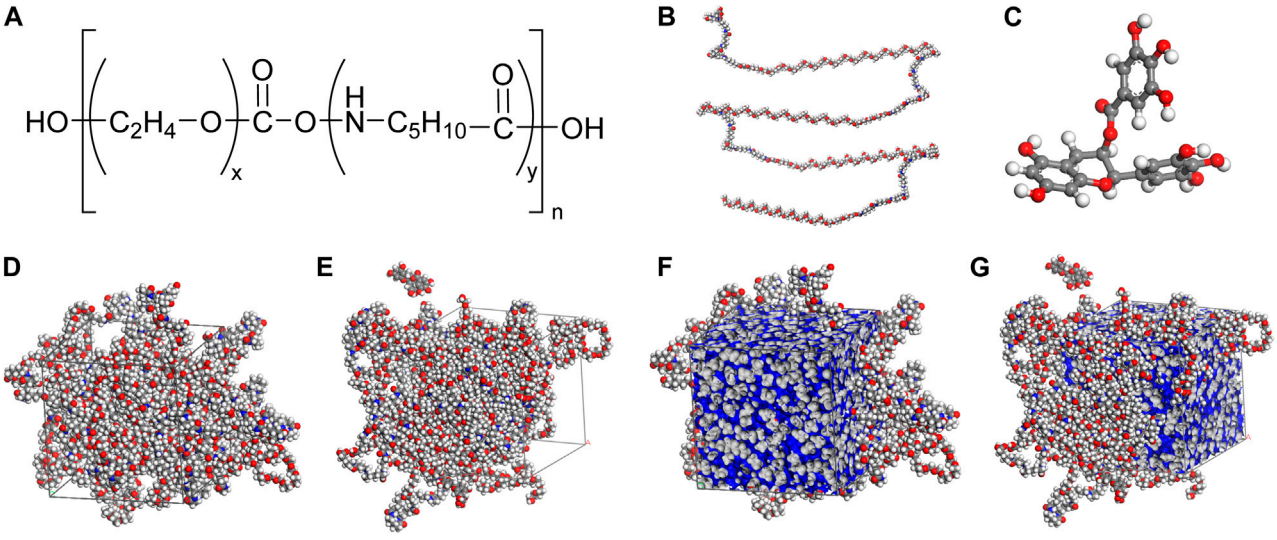

FIGURE 5
(a) Pebax chain consisting of PEO unit (x = 35), and PA unit (y = 9) with repeating unit of 4 (n = 4). Simulated **(b)** Pebax chain, **(c)** EGCG molecule, **(d)** Pebax cell consisting of 5 Pebax chains, **(e)** Pebax/EGCG 5% cell consisting of 5 Pebax chains and 6 EGCG molecules, simulated free volume of **(f)** Pebax cell and **(g)** Pebax/EGCG 5% cell.

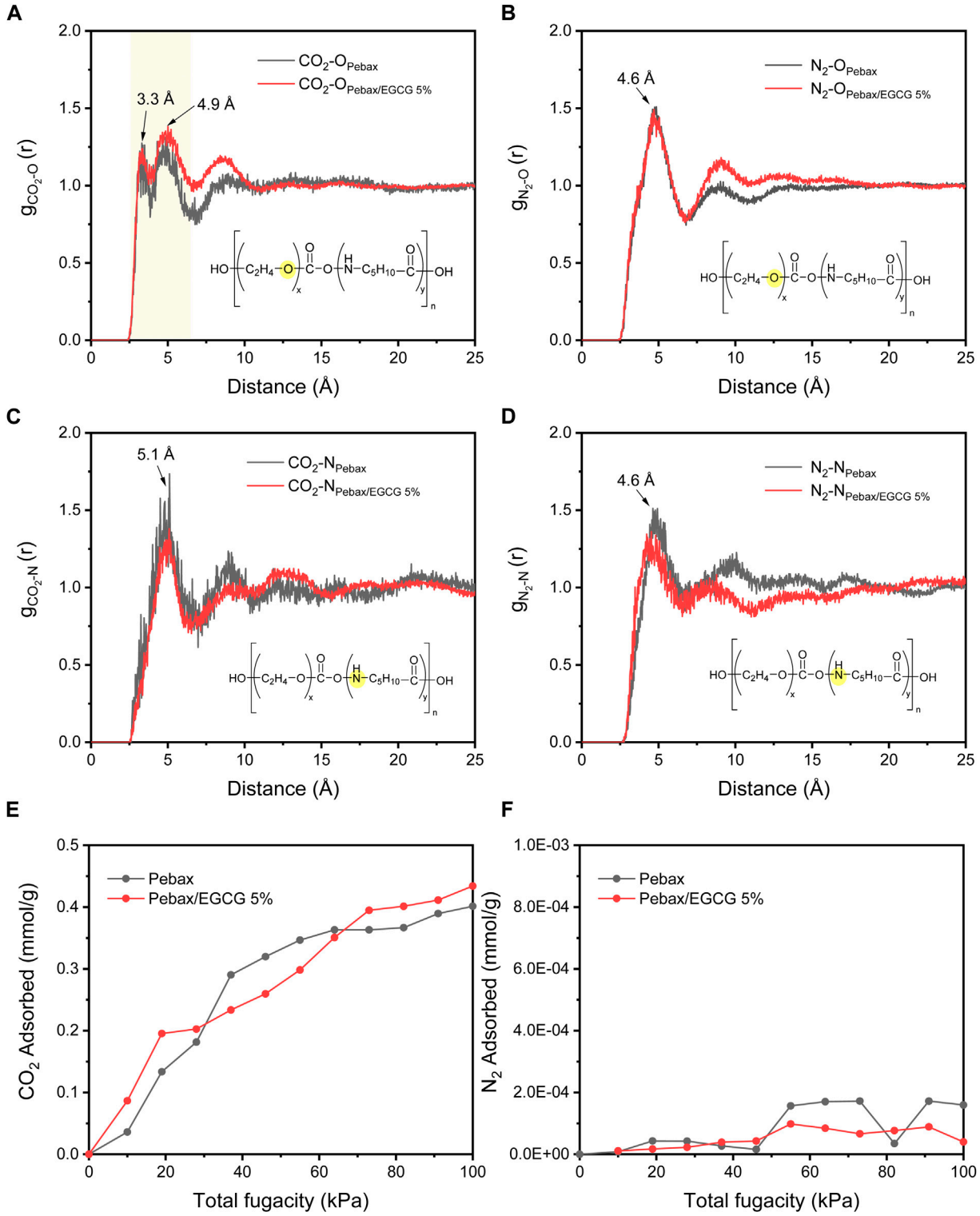

FIGURE 6
RDF profiles of **(a)** CO_2-O **(b)** N_2-O, **(c)** CO_2-N, and **(d)** N_2-N pairs. Simulated **(e)** CO_2 and **(f)** N_2 adsorption isotherms of neat Pebax and Pebax/EGCG 5% membranes.

membranes revealed dense and uniform structures, with no visible defects. This defect-free morphology is critical for ensuring the membranes' effectiveness in gas separation applications. These observations confirm that the incorporation of EGCG maintains the structural integrity of the membranes while influencing their microstructural characteristics.

3.3 Gas separation performance of membranes

The pure gas permeability and selectivity of the Pebax/EGCG membranes were measured at 35°C and 1 bar using the time-lag method, with results presented in Figure 4a and Table 3. The neat Pebax membrane exhibited a CO_2 permeability of 71.7 Barrer and a CO_2/N_2 selectivity of 37.2. This performance is attributed to the structural characteristics of Pebax, where the PEO segment enhances CO_2 solubility, improving selectivity against non-polar gases, while the crystalline PA domain restricts gas diffusion, thereby lowering overall permeability. With increasing EGCG content, distinct trends in gas separation performance were observed. At 5 wt% EGCG loading, the CO_2 permeability decreased to 60.2 Barrer, while the CO_2/N_2 selectivity increased significantly to 49.6, representing more than a 30% improvement over the neat Pebax membrane.

The enhancement in selectivity is attributed to two key factors: (1) increased CO_2 diffusivity selectivity due to a reduction in free volume, resulting from hydrogen-bond-induced densified structure of Pebax chains, and (2) enhanced CO_2 solubility selectivity caused by the greater exposure of amorphous PEO chains, facilitated by hydrogen-bond interactions with EGCG. Gravimetric CO_2 sorption analysis (Supplementary Figure S5) confirmed the improved CO_2 solubility of Pebax/EGCG 5% compared to neat Pebax. At a constant temperature of 27°C, the Pebax/EGCG 5% membrane exhibited a significantly higher CO_2 uptake, highlighting the role of EGCG in promoting solubility. However, higher EGCG loadings negatively impacted performance. Excessive EGCG led to increased hydrogen bonding between EGCG molecules, reducing interchain interactions within Pebax. This disrupted the selective permeation of CO_2 through the PEO domains, resulting in a decline in both permeability and selectivity. At 20 wt% EGCG loading, the CO_2 permeability dropped to 2.6 Barrer, and the CO_2/N_2 selectivity decreased to 34.9. These results indicate that 5 wt% EGCG is the optimal loading level, where the permeability reduction caused by hydrogen bonding remains minimal, and the selectivity enhancement is maximized. In Figure 4b and Supplementary Table S1, the CO_2/N_2 separation performance of the Pebax/EGCG membranes is compared to previously reported all-polymeric, PEO-based crosslinked or H-bonded membranes for CO_2 separation (Oh et al., 2025; Kim et al., 2020; Norouzbahari and Gharibi, 2020; Li et al., 2024; Chen et al., 2023; Wang et al., 2023; Choi and Kang, 2016; Yoon and Kang, 2018; Nobakht and Abedini, 2022a). Only a few of the reported hydrogen-bonded membranes exceed the 2008 upper limit (Nobakht and Abedini, 2022a).

In comparison to chemically crosslinked PEO-based membranes, such as UV crosslinked PEO (CO_2 permeablity of 223 Barrer, CO_2/N_2 selectivity of 47) and thiol-modified copolymer membranes (CO_2 permeablity of 128 Barrer, CO_2/N_2 selectivity of 64), the Pebax/EGCG membrane achieves comparable or superior selectivity while maintaining a relatively simple fabrication process without the need for chemical crosslinking. Additionally, when benchmarked against hydrogen-bond-induced membranes, such as PEO/trehalose (CO_2 permeablity of 117 Barrer, CO_2/N_2 selectivity of 51) and PEO/5-hydroxyisophthalic acid (CO_2 permeablity of 573 Barrer, CO_2/N_2 selectivity of 32.4), the Pebax/EGCG membrane demonstrates a favorable balance between permeability and selectivity. Furthermore, while polyalcohol-blended Pebax membranes (e.g., Pebax/maltitol, CO_2 permeablity of 341 Barrer, CO_2/N_2 selectivity of 66.65) exhibit higher permeability, they require significantly higher operating pressures (10 bar), whereas the Pebax/EGCG membranes achieve enhanced selectivity under mild conditions (1 bar). Among both the Pebax and Pebax/EGCG membranes, the Pebax/EGCG 5% membrane demonstrates the most promising performance. This membrane will be further developed into a thin-film composite membrane to assess its scalability for practical applications.

3.4 MD simulation

The simulated models of Pebax, EGCG, Pebax cell, and Pebax/EGCG 5% cell are shown in Figure 5. Thermodynamic and physical equilibrium conditions of each model were confirmed (Supplementary Figure S6). The final snapshots of each simulation cell from the molecular dynamics simulations were used to calculate the fractional free volume (FFV) of the Pebax and Pebax/EGCG 5% cells. The FFV was determined using the following method (Salestan et al., 2021):

$$FFV_{sim} = \frac{V\text{-}V_0}{V};\ V_0 = 1.3 \times V_{vdw}$$

where V is the total volume of the simulation cell and V_{vdw} is the van der Waals volume computed with atom volumes and surfaces task in Materials Studio 2024 using a Connolly radius of 0 Å and a van der Waals scale factor of 1. The simulated density (1.14 g/cm^3) and FFV (0.138) of Pebax closely align with the experimental values (1.14 g/cm^3, 0.12–0.13) (Shin et al., 2019; Sharma et al., 2019), confirming the accuracy of the chosen repeating unit. The Pebax/EGCG 5% membrane exhibited a slightly higher density (1.15) and lower FFV (0.134) compared to Pebax, which accounts for its reduced gas permeability.

Radial distribution functions (RDFs, Figures 6a–d) were used to analyze CO_2 and N_2 distribution around functional atoms in Pebax and Pebax/EGCG 5% membranes. The RDFs of CO_2 around PEO oxygen ($g_{CO_2-O}(r)$) and PA nitrogen ($g_{CO_2-N}(r)$), and N_2 around PEO oxygen ($g_{N_2-O}(r)$) and PA nitrogen ($g_{N_2-N}(r)$), were analyzed to assess changes in gas-functional group interactions in Pebax with EGCG incorporation. $g_{CO_2-O}(r)$ exhibited a two-layer conformation with a first maximum at 3.3 Å, whereas $g_{CO_2-N}(r)$, $g_{N_2-O}(r)$, and $g_{N_2-N}(r)$ showed first maximums at 4.6–5.1 Å, indicating that the Coulombic interaction is only present in CO_2-O (Xu et al., 2011). The stronger CO_2-O bonding in Pebax/EGCG 5%, indicated by higher peak intensities in $g_{CO_2-O}(r)$ (Xu et al., 2011), suggests enhanced CO_2 solubility in Pebax/EGCG 5% membrane compared to neat Pebax. Gas sorption simulations (Figures 6e, f) using the Metropolis Monte Carlo method revealed higher CO_2 loading and lower N_2 loading in Pebax/EGCG 5%, consistent with the experimental CO_2 sorption results (Supplementary Figure S5). This indicates enhanced solubility selectivity in Pebax/EGCG 5% compared to neat Pebax. Overall, the MD simulation results align with the experimental data, showing a reduced FFV (indicating lower diffusivity) and increased CO_2 solubility in Pebax/EGCG 5% relative to neat Pebax.

4 Conclusion

This study presents a comprehensive analysis of the structural, thermal, mechanical, and gas separation properties of all-organic,

H-bonded Pebax/EGCG membranes, highlighting their potential for CO_2 separation applications. Detailed physicochemical analyses demonstrated that the hydroxyl groups of EGCG effectively interact with the Pebax matrix through H-bonding, which disrupts the crystalline structure of the PA domains and exposes the amorphous PEO chains. This structural modification significantly influences the membrane's gas separation performance. MD simulations supported these findings, confirming the changes in sorption behaviors with EGCG incorporation. At low EGCG loadings, H-bond-induced crosslinking between Pebax chains and amorphous PEO segments reduces the FFV, enhancing both CO_2/N_2 diffusivity selectivity and solubility selectivity. The membrane with an optimal EGCG loading of 5 wt% achieved a CO_2 permeability of 60.2 Barrer and a CO_2/N_2 selectivity of 49.6 (133% of neat Pebax). This balance of properties demonstrates the effective tuning of the Pebax membrane structure through controlled H-bond interaction. However, excessive EGCG loading (20 wt%) led to overly strong interactions and a densified structure, causing a significant reduction in CO_2 permeability (3.6% of neat Pebax) and selectivity (94% of neat Pebax), highlighting the importance of optimizing the additive concentration. In conclusion, the study establishes 5 wt% EGCG as the ideal concentration for Pebax membranes, achieving a balance between flexibility, structural integrity, and enhanced gas separation performance. This work highlights the innovative use of EGCG as an H-bond inducer to fine-tune membrane properties, offering a promising strategy for developing advanced materials for CO_2 separation. Future work will focus on transforming the freestanding membrane into a thin-film composite membrane to evaluate its industrial viability, paving the way for practical applications in carbon capture technologies.

Data availability statement

The original contributions presented in the study are included in the article/Supplementary Material, further inquiries can be directed to the corresponding author.

Author contributions

JH: Conceptualization, Data curation, Writing–original draft. MK: Conceptualization, Data curation, Writing–original draft. NO: Data curation, Writing–original draft. JK: Conceptualization, Supervision, Writing–review and editing.

Funding

The author(s) declare that financial support was received for the research, authorship, and/or publication of this article. This work was supported by the National Research Foundation (NRF) of South Korea, funded by the Ministry of Science and ICT (RS-2024-00333678, RS-2024-00467234).

Conflict of interest

The authors declare that the research was conducted in the absence of any commercial or financial relationships that could be construed as a potential conflict of interest.

The author(s) declared that they were an editorial board member of Frontiers, at the time of submission. This had no impact on the peer review process and the final decision.

Generative AI statement

The author(s) declare that no Generative AI was used in the creation of this manuscript.

Publisher's note

All claims expressed in this article are solely those of the authors and do not necessarily represent those of their affiliated organizations, or those of the publisher, the editors and the reviewers. Any product that may be evaluated in this article, or claim that may be made by its manufacturer, is not guaranteed or endorsed by the publisher.

Supplementary material

The Supplementary Material for this article can be found online at: https://www.frontiersin.org/articles/10.3389/frmst.2025.1541236/full#supplementary-material

References

Chen, Y., He, M., Zhang, J., Su, Y., Xue, Z., He, C., et al. (2023). Design of ultrathin cross-linked poly(ethylene oxide) selective layer for high-performance CO2 capture. *Chem. Eng. J.* 478 147530. doi:10.1016/j.cej.2023.147530

Choi, Y., and Kang, S. W. (2016). Effect of 4-hydroxybenzoic acid on CO2 separation performance of poly(ethylene oxide) membrane. *Macromol. Res.* 24 (12), 1111–1114. doi:10.1007/s13233-016-4154-x

Didden, J., Thür, R., Volodin, A., and Vankelecom, I. F. J. (2018). Blending PPO-based molecules with Pebax MH 1657 in membranes for gas separation. *J. Appl. Polym. Sci.* 135(27) 46433. doi:10.1002/app.46433

Embaye, A. S., Martínez-Izquierdo, L., Malankowska, M., Téllez, C., and Coronas, J. (2021). Poly (ether-block-amide) copolymer membranes in CO2 separation applications. *Energy and fuels* 35 (21), 17085–17102. doi:10.1021/acs.energyfuels.1c01638

Erpenbeck, J. J., and Wood, W. W. (1991). Self-diffusion coefficient for the hard-sphere fluid. *Phys. Rev. A* 43 (8), 4254–4261. doi:10.1103/PhysRevA.43.4254

Farashi, Z., Azizi, S., Arzhandi, M.R.-D., Noroozi, Z., and Azizi, N. (2019). Improving CO2/CH4 separation efficiency of Pebax-1657 membrane by adding Al2O3 nanoparticles in its matrix. *J. Nat. Gas Sci. Eng.* 72, 103019. doi:10.1016/j.jngse.2019.103019

Gao, X., Qi, S., Yang, B., Su, Y., Li, J., and Wang, D. (2021). Synergistic effect of plasticizer and nucleating agent on crystallization behavior of polylactide during fused filament fabrication. *Polymer* 215 123426. doi:10.1016/j.polymer.2021.123426

Guiver, M. D. (2022). Field grand challenge for membrane science and Technology. *Front. Membr. Sci. Technol.* 1, 878879. doi:10.3389/frmst.2022.878879

Han, Y., and Ho, W. S. W. (2021). Polymeric membranes for CO2 separation and capture. *J. Membr. Sci.* 628 119244. doi:10.1016/j.memsci.2021.119244

Hansen, J. P., and McDonald, I. R. (1990). *Theory of simple liquids*. Academic Press1990.

Hao, L., Li, P., and Chung, T.-S. (2014). PIM-1 as an organic filler to enhance the gas separation performance of Ultem polyetherimide. *J. Membr. Sci.* 453, 614–623. doi:10.1016/j.memsci.2013.11.045

Hou, L., Wang, Z., Chen, Z., Chen, W., and Yang, C. (2020). PIM-1 as an organic filler to enhance CO2 separation performance of poly (arylene fluorene ether ketone). *Sep. Purif. Technol.* 242, 116766. doi:10.1016/j.seppur.2020.116766

Hyo Jun, M., Young Jae, S., and Jong Hak, K. (2024). Polymeric additive influence on the structure and gas separation performance of high-molecular-weight PEO blend membranes. *Membr. J.* 34 (3), 192–203. doi:10.14579/membrane_journal.2024.34.3.192

Kang, M., Min, H. J., Kim, N. U., and Kim, J. H. (2021). Amphiphilic micelle-forming PDMS-PEGBEM comb copolymer self-assembly to tailor the interlamellar nanospaces of defective poly(ethylene oxide) membranes. *Sep. Purif. Technol.* 257 117892. doi:10.1016/j.seppur.2020.117892

Kargari, A., and Rezaeinia, S. (2020). State-of-the-art modification of polymeric membranes by PEO and PEG for carbon dioxide separation: a review of the current status and future perspectives. *J. Industrial Eng. Chem.* 84 1–22. doi:10.1016/j.jiec.2019.12.020

Kim, J. H. (2022). Grand challenges in membrane applications—gas and vapor. *Front. Membr. Sci. Technol.* 1, 853402. doi:10.3389/frmst.2022.853402

Kim, N. U., Park, B. J., Guiver, M. D., and Kim, J. H. (2020). Use of non-selective, high-molecular-weight poly(ethylene oxide) membrane for CO2 separation by incorporation of comb copolymer. *J. Membr. Sci.* 605 118092. doi:10.1016/j.memsci.2020.118092

Kim, N. U., Park, B. J., Park, M. S., Park, J. T., and Kim, J. H. (2019). Semi-interpenetrating polymer network membranes based on a self-crosslinkable comb copolymer for CO2 capture. *Chem. Eng. J.* 360, 1468–1476. doi:10.1016/j.cej.2018.10.152

Kim, Y. J., Lee, S. Y., Kang, D. R., Kim, J.-H., and Kim, J. H. (2024). Immiscibility-induced phase-separated PEBAX membranes embedded with PTFE particles: simultaneously enhanced permeability and selectivity, *J. Membr. Sci.* 701 122746. doi:10.1016/j.memsci.2024.122746

Knebel, A. A., and Caro, J. (2022). Metal–organic frameworks and covalent organic frameworks as disruptive membrane materials for energy-efficient gas separation. *Nat. Nanotechnol.* 17 (9), 911–923. doi:10.1038/s41565-022-01168-3

Lei, L., Bai, L., Lindbråthen, A., Pan, F., Zhang, X., and He, X. (2020). Carbon membranes for CO2 removal: status and perspectives from materials to processes. *Chem. Eng. J.* 401 126084. doi:10.1016/j.cej.2020.126084

Li, R., Yang, Y., Zhang, Z., Lian, S., and Song, C. (2024). Imine-linked polymer derived N-Doped microporous carbons in PEO-based mixed matrix membranes for enhanced CO2/N2 separation: a comparative study. *J. Membr. Sci.* 690 122203. doi:10.1016/j.memsci.2023.122203

Liu, S. L., Shao, L., Chua, M. L., Lau, C. H., Wang, H., and Quan, S. (2013). Recent progress in the design of advanced PEO-containing membranes for CO2 removal, *Prog. Polym. Sci.* 38(7) 1089–1120. doi:10.1016/j.progpolymsci.2013.02.002

Liu, T. X., Liu, Z. H., Ma, K. X., Shen, L., Zeng, K. Y., and He, C. B. (2003). Morphology, thermal and mechanical behavior of polyamide 6/layered-silicate nanocomposites, *Compos. Sci. Technol.* 63(3) 331–337. doi:10.1016/S0266-3538(02)00226-9

Liu, Y., Wu, H., Wu, S., Song, S., Guo, Z., Ren, Y., et al. (2021). Multifunctional covalent organic framework (COF)-Based mixed matrix membranes for enhanced CO2 separation. *J. Membr. Sci.* 618 118693. doi:10.1016/j.memsci.2020.118693

Mohammed, S. A., Nasir, A. M., Aziz, F., Kumar, G., Sallehhudin, W., Jaafar, J., et al. (2019). CO2/N2 selectivity enhancement of PEBAX MH 1657/Aminated partially reduced graphene oxide mixed matrix composite membrane. *Sep. Purif. Technol.* 223, 142–153. doi:10.1016/j.seppur.2019.04.061

Nobakht, D., and Abedini, R. (2022a). Improved gas separation performance of Pebax®1657 membrane modified by poly-alcoholic compounds, *J. Environ. Chem. Eng.* 10(3) 107568. doi:10.1016/j.jece.2022.107568

Nobakht, D., and Abedini, R. (2022b). Improved gas separation performance of Pebax® 1657 membrane modified by poly-alcoholic compounds. *J. Environ. Chem. Eng.* 10 (3), 107568. doi:10.1016/j.jece.2022.107568

Norouzbahari, S., and Gharibi, R. (2020). UV cross-linked poly(ethylene glycol)-based membranes with different fractional free volumes for CO2 capture: synthesis, characterization, and thiol-ene modification evaluation. *Ind. Eng. Chem. Res.* 59 (13), 6078–6089. doi:10.1021/acs.iecr.9b06193

Oh, N. Y., Ko, Y., Kim, K. C., Cho, H., Kwak, H., and Kim, J. H. (2025). Low-cost, all-organic, hydrogen-bonded thin-film composite membranes for CO2 capture: experiments and molecular dynamic simulations, *J. Membr. Sci.* 713 123307. doi:10.1016/j.memsci.2024.123307

Pan, J., Li, M., Zhang, S., Jiang, Y., Lv, Y., Liu, J., et al. (2019). Effect of epigallocatechin gallate on the gelatinisation and retrogradation of wheat starch. *Food Chem.* 294, 209–215. doi:10.1016/j.foodchem.2019.05.048

Rabiee, H., Ghadimi, A., Abbasi, S., and mohammadi, T. (2015). CO2 separation performance of poly (ether-b-amide6)/PTMEG blended membranes: permeation and sorption properties. *Chem. Eng. Res. Des.* 98, 96–106. doi:10.1016/j.cherd.2015.03.026

Ren, S., Hou, Y., Wu, W., Tian, S., and Liu, W. (2012). CO2 capture from flue gas at high temperatures by new ionic liquids with high capacity. *RSC Adv.* 2 (6), 2504–2507. doi:10.1039/C2RA00996J

Salestan, S. K., Rahimpour, A., and Abedini, R. (2021). Experimental and theoretical studies of biopolymers on the efficient CO2/CH4 separation of thin-film Pebax®1657 membrane, *Chem. Eng. Process. - Process Intensif.* 163 108366. doi:10.1016/j.cep.2021.108366

Shao, L., and Chung, T.-S. (2009). *In situ* fabrication of cross-linked PEO/silica reverse-selective membranes for hydrogen purification, *Int. J. Hydrogen Energy* 34(15) 6492–6504. doi:10.1016/j.ijhydene.2009.05.137

Sharma, P., Kim, Y.-J., Kim, M.-Z., Alam, S. F., and Cho, C. H. (2019). A stable polymeric chain configuration producing high performance PEBAX-1657 membranes for CO2 separation. *Nanoscale Adv.* 1 (7), 2633–2644. doi:10.1039/C9NA00170K

Shin, J. E., Lee, S. K., Cho, Y. H., and Park, H. B. (2019). Effect of PEG-MEA and graphene oxide additives on the performance of Pebax®1657 mixed matrix membranes for CO2 separation. *J. Membr. Sci.* 572 300–308. doi:10.1016/j.memsci.2018.11.025

Sun, W., Chen, X., Wu, L., Hu, Y., and Zhang, W. (2023). Analysis of the distribution and influencing factors of diffusion coefficient model parameters based on molecular dynamics simulations. *ACS Omega* 8 (25), 22536–22544. doi:10.1021/acsomega.3c00754

Thanakkasaranee, S., Kim, D., and Seo, J. (2018). Preparation and characterization of poly (ether-block-amide)/polyethylene glycol composite films with temperature-dependent permeation. *Polymers* 10 (2), 225. doi:10.3390/polym10020225

Thankamony, R. L., Li, X., Das, S. K., Ostwal, M. M., and Lai, Z. (2019). Porous covalent triazine piperazine polymer (CTPP)/PEBAX mixed matrix membranes for CO2/N2 and CO2/CH4 separations, *J. Membr. Sci.* 591 117348. doi:10.1016/j.memsci.2019.117348

Wang, D., Kim, D., Shin, C.-H., Zhao, Y., Park, J.-S., and Ryu, M. (2019). Evaluation of epigallocatechin gallate (EGCG) to remove Pb (II) using spectroscopic and quantum chemical calculation method. *Environ. Earth Sci.* 78, 138–8. doi:10.1007/s12665-019-8127-1

Wang, Z.-X., Zhang, W.-H., Yu, G., Yin, M.-J., Li, S., and An, Q.-F. (2023). Defect-free PEO membrane fabrication by hydrogen bonding coupling thermal annealing for carbon capture, *Chem. Eng. Sci.* 282 119354. doi:10.1016/j.ces.2023.119354

Wu, D., Hou, R., Yi, C., Smith, S. J. D., Fu, J., Ng, D., et al. (2021). Enhancing polyimide-based mixed matrix membranes performance for CO2 separation containing PAF-1 and p-DCX, *Sep. Purif. Technol.* 268 118677. doi:10.1016/j.seppur.2021.118677

Xu, M., Chen, J., Zhang, C., Du, Z., and Mi, J. (2011). A theoretical study of structure–solubility correlations of carbon dioxide in polymers containing ether and carbonyl groups. *Phys. Chem. Chem. Phys.* 13 (47), 21084–21092. doi:10.1039/C1CP22671A

Yan, W., Huang, H., Zhang, A., Dong, H., Liao, W., He, Z., et al. (2024). Frontiers in applications of porous materials in CO2 gas separation membranes: mechanisms, membrane properties, and future perspectives of porous aromatic frameworks (PAFs). *J. Environ. Chem. Eng.* 12(5) 113509. doi:10.1016/j.jece.2024.113509

Yeh, Y.-J., Lin, W., Chiang, W.-H., and Tung, K.-L., (2023). Plasma-engineered graphene quantum dot-based nanocomposites as smart CO2-philic membranes with extremely high separation performance. *Chem. Eng. J.* 476 146547. doi:10.1016/j.cej.2023.146547

Yin, H.-Y., Wei, X.-F., Bao, R.-Y., Dong, Q.-X., Liu, Z.-Y., Yang, W., et al. (2015). Enhancing thermomechanical properties and heat distortion resistance of poly(l-lactide) with high crystallinity under high cooling rate. *ACS Sustain. Chem. and Eng.* 3 (4), 654–661. doi:10.1021/sc500783s

Yoon, K. W., and Kang, S. W. (2018). Highly permeable and selective CO2 separation membrane to utilize 5-hydroxyisophthalic acid in poly(ethylene oxide) matrix, *Chem. Eng. J.* 334 1749–1753. doi:10.1016/j.cej.2017.11.113

Yu, S., An, S. J., Kim, K. J., Lee, J. H., and Chi, W. S. (2023). High-loading poly(ethylene glycol)-blended poly(acrylic acid) membranes for CO2 separation. *ACS Omega* 8 (2), 2119–2127. doi:10.1021/acsomega.2c06143

Zhu, B., Jiang, X., He, S., Yang, X., Long, J., Zhang, Y., et al. (2020). Rational design of poly (ethylene oxide) based membranes for sustainable CO 2 capture. *J. Mater. Chem. A* 8 (46), 24233–24252. doi:10.1039/d0ta08806d

Zou, X., and Zhu, G. (2018). Microporous organic materials for membrane-based gas separation. *Adv. Mater.* 30 (3), 1700750. doi:10.1002/adma.201700750